Supplementary Information

Computational exploration of chemically ordered and disordered M-sites in $M'_2M''B_2$ and $M'_4M''B_3$ compounds

Adam Carlsson, Rodrigo Mantovani Ronchi, Johanna Rosen, Martin Dahlqvist
Materials Design, Department of Physics, Chemistry and Biology (IFM),
Linköping University, SE-581 83 Linköping, Sweden
Corresponding author: martin.dahlqvist@liu.se

SQS convergence

The disordered structures used herein modeled by SQS structures to simulate solid solution on the M-sites were derived through a convergence of the energy when increasing the cell size. Below is the convergence for the *P*4/*mbm* ($M'_2M''B_2$ prototype) and *I*4/*mcm* ($M'_4M''B_3$ prototype) structures where the energy is displayed as ΔE_0 which is the energy with respect to the energy of the largest cell size. The convergence was performed for the M' = Cr and M'' = W to replicate the scenario in Ref. [1].

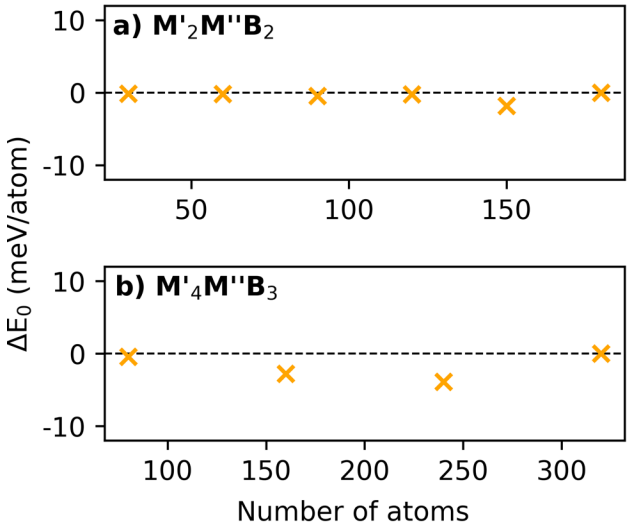

Figure S1. Energy convergence with respect to the energy of the cell with the greatest size for the SQS structures with disordered M-sites versus the number of atoms of the generated supercell.

The energy difference with respect to the cell of the greatest number, ΔE_0, is seen to vary and remain constant for both considered symmetries as the cells are increased. The *P4/mbm* symmetry yielded an energy difference of 0.4 meV/atom when occupied by 90 atoms which was the considered cell for further analysis. Similarly, the cell with 80 atoms yielded the same energy as the cell with 320 atoms for the I4/mbm symmetry.

Complete phase stability for $M'_2M''B_2$

Complete heatmap for the $M'_2M''B_2$ composition with M' and M'' being occupied by elements ranging from period 3 to 6 arranged after their atomic number. The colors range from red (metastable) to blue (stable) whereas grey illustrates phases with ΔH_{cp} > 150 meV/atom. The symbols of the elements illustrate the arrangement of the M-sublattice with a filled representing ordered and unfilled disordered. Experimentally known phases are distinguished by a black edge and phases deemed uncertain with a grey square.

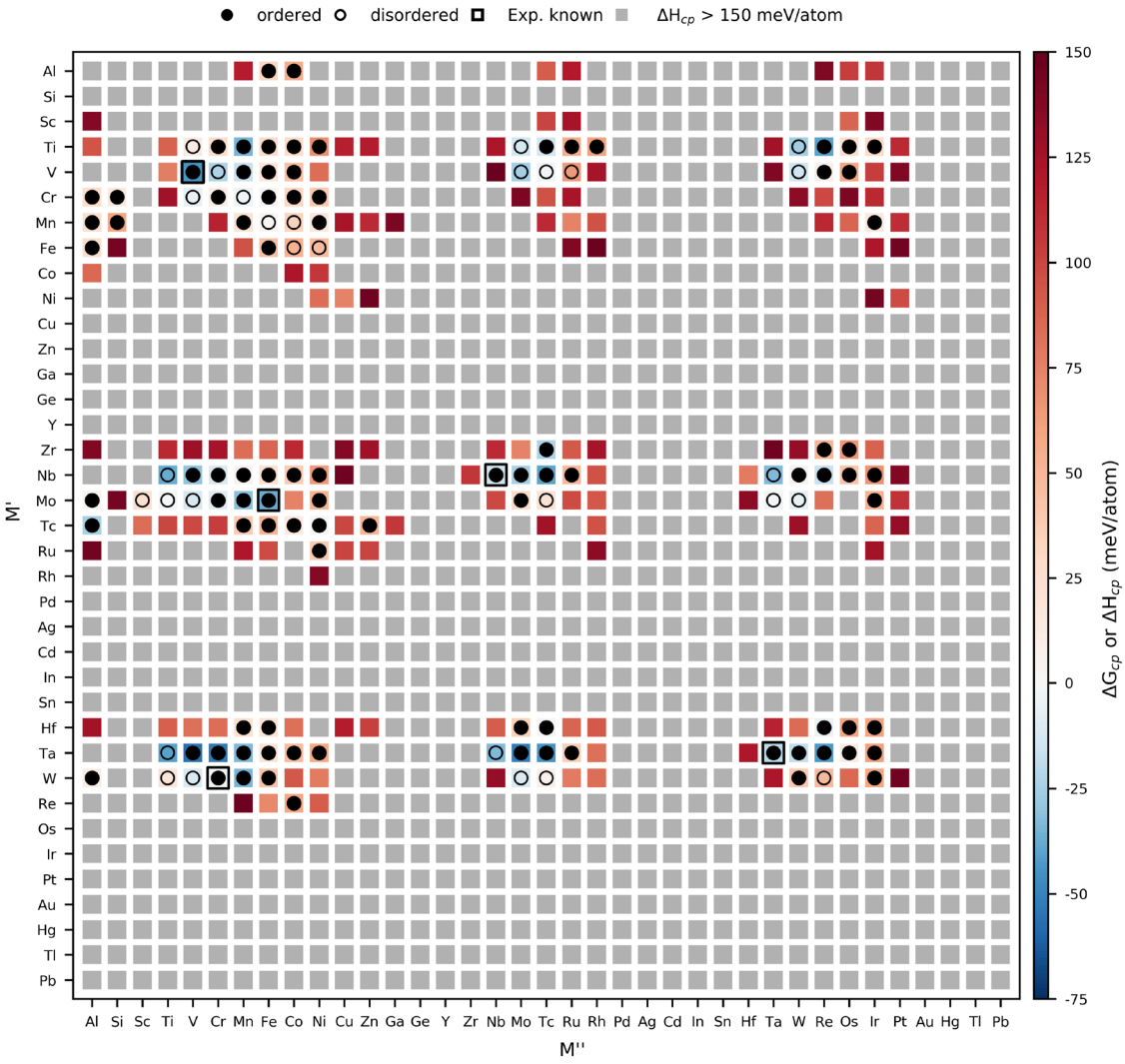

Figure S2. Complete phase stability heatmap at 2000 K where stability is depicted as the color ranging from red (metastable) to blue (stable). Phases with ΔH_{cp} > 150 meV/atom are colored grey and denoted unstable.

Table S1. Gibb's free energy, M' and M'' arrangement and the set of most of the competing phases for the predicted stable $M'_2M''B_2$ phases with symmetry *P4/mbm* are displayed in Figure 2 at 2000 K.

M'	M''	ΔH_{cp} or ΔG_{cp} (meV/atom)	M' and M'' arrangement	Set of most competing phases
Ta	V	-56.8318	Ordered	$Ta_3B_2 + V_3B_2$
Ta	Cr	-53.7503	Ordered	Cr + TaB
Ta	Mo	-52.6921	Ordered	Mo + TaB
Ta	Tc	-44.9297	Ordered	Tc_7B_3 + TaTc + TaB
V	V	-44.5126	Ordered	VB + V
Ta	Re	-43.1232	Ordered	Re + TaB
Ti	Re	-40.9885	Ordered	ReTi + TiB_2
Ta	Ti	-40.6692	Disordered	$Ta_3TiB_4 + Ta_3B_2$ + Ti
Nb	Tc	-40.4089	Ordered	Tc + NbB
Nb	Ti	-37.9343	Disordered	$NbTiB_2$ + Nb
Mo	Fe	-37.2176	Ordered	$FeMo_4B_3 + Fe_2B$ + MoB
Ti	Mn	-34.807	Ordered	$Ti_3B_4 + Mn_2Ti$
W	Mn	-34.7966	Ordered	$Mn_3WB_4 + MnW_4B_3 + Mn_2B$
Ta	Mn	-33.8266	Ordered	$Mn_2Ta + Mn_2B$ + TaB
Ta	Nb	-33.0403	Disordered	$Ta_3B_2 + Nb_2TaB_2$
Nb	Ta	-32.8848	Disordered	$Nb_3B_2 + NbTa_2B_2$
Mo	Mn	-31.1031	Ordered	$MnMo_4B_3$ + MoB + Mn_2B
Nb	V	-30.1405	Ordered	$Nb_3B_2 + V_3B_2$
Ti	W	-26.2655	Disordered	TiB + W
V	Mo	-25.7328	Disordered	Mo + VB
Tc	Al	-25.0545	Ordered	$Al_4Tc + AlTc_2 + TcB_2$
Nb	Mo	-24.8286	Ordered	Mo + NbB
V	Cr	-23.3763	Disordered	$Cr_3V_9B_8 + Cr_2VB_2$
Zr	Tc	-23.3644	Ordered	Zr + Tc_2Zr + ZrB_2
Ta	Ta	-20.4912	Ordered	Ta + TaB
Ta	W	-18.534	Ordered	TaB + W
V	Mn	-16.9839	Ordered	Mn_2B + MnV + VB
Nb	Re	-16.9464	Ordered	Re + NbB
Nb	Nb	-14.7118	Ordered	Nb + NbB
V	W	-14.3244	Disordered	VB + W
Ti	Tc	-14.0164	Ordered	TcTi + TiB_2
Ti	Mo	-13.2575	Disordered	Ti_3B_4 + TiB + Mo_3Ti
Mo	V	-12.8257	Disordered	$MoV_2B_2 + Mo_4VB_3$ + MoB
W	V	-11.4814	Disordered	VW_4B_3 + VB
W	Mo	-11.3594	Disordered	MoW_4B_3 + MoB
Nb	Cr	-11.1174	Ordered	Cr + NbB
Mo	Cr	-8.22328	Ordered	$CrMo_4B_3$ + CrB
Mo	W	-5.43422	Disordered	MoB + W
Cr	V	-5.29457	Disordered	Cr_4VB_3 + VB
Hf	Re	-3.69273	Ordered	$Hf_9Re_4B + Hf_{21}Re_{25} + HfB_2$
W	Cr	-2.91818	Ordered	CrW_4B_3 + CrB
Cr	Mn	-2.78801	Disordered	Cr_4MnB_3 + CrB + Mn_2B
V	Tc	-2.15403	Disordered	Tc_7B_3 + TcV + VB
Mo	Ta	-1.64373	Disordered	$MoTa_2B_2$ + Mo + MoB
Mo	Ti	-1.04939	Disordered	$MoTiB_2$ + Mo

Figure S3 to S27 shows phonon dispersion spectrum for stable $M'_2M''B_2$ phases with symmetry *P4/mbm* and with M' and M'' being ordered. Note that Tc-based phases have intentionally been left out since Tc is very unstable and can only be made artificially. The absence of imaginary frequencies indicates that the ordered MAB phase is dynamically stable. One $M'_2M'''B_2$ phases is found dynamically unstable, i.e., Ta_2MnAlB_2, whereas the other 25 are dynamically stable.

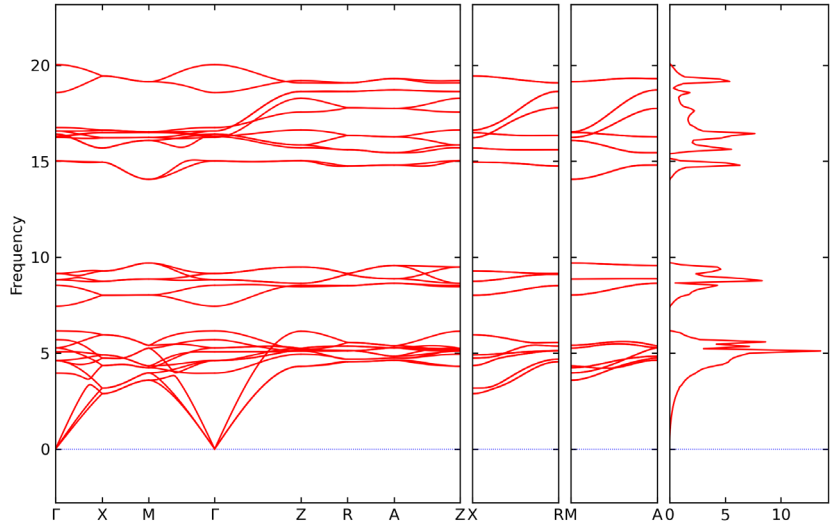

Figure S3. Phonon dispersion spectra and phonon DOS for Ta_2VB_2.

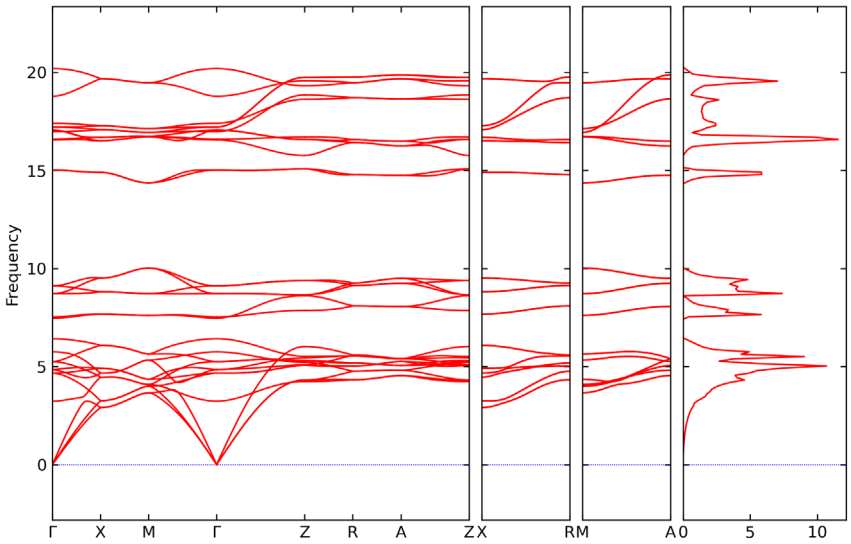

Figure S4. Phonon dispersion spectra and phonon DOS for Ta_2CrB_2.

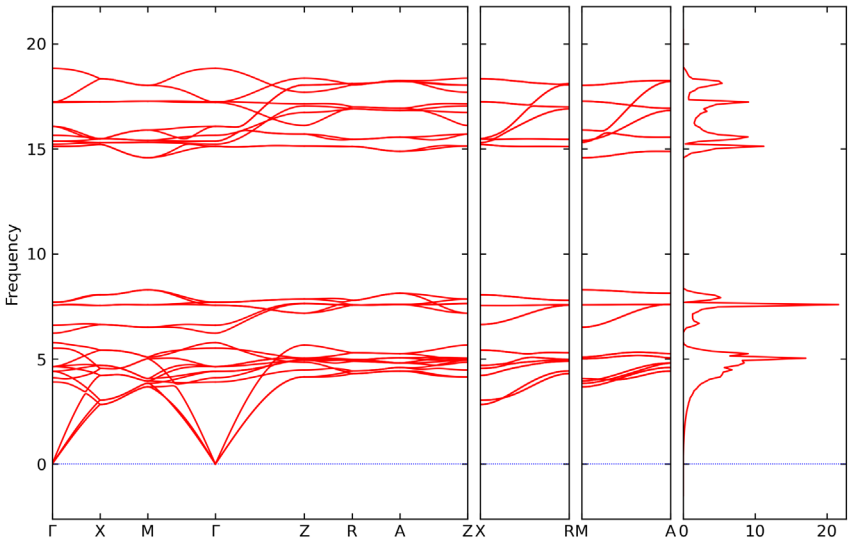

Figure S5. Phonon dispersion spectra and phonon DOS for Ta_2MoB_2.

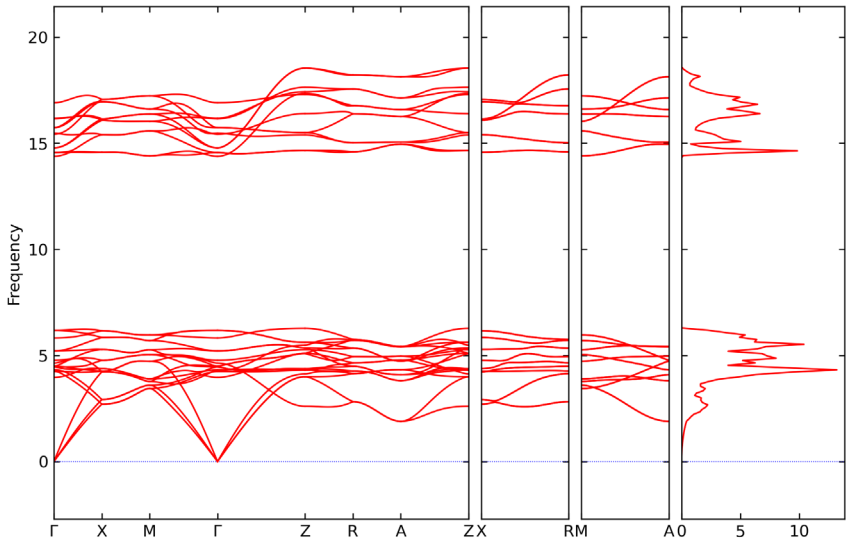

Figure S6. Phonon dispersion spectra and phonon DOS for Ta_2ReB_2.

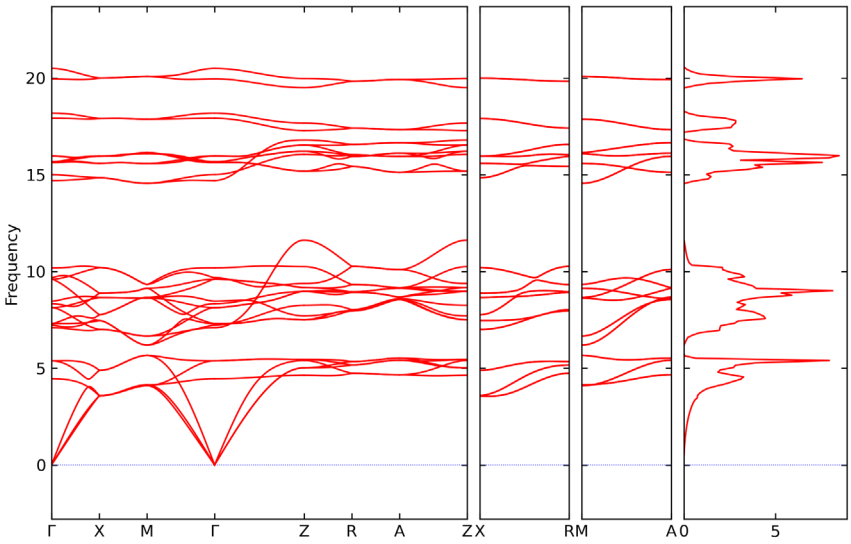

Figure S7. Phonon dispersion spectra and phonon DOS for Ti_2ReB_2.

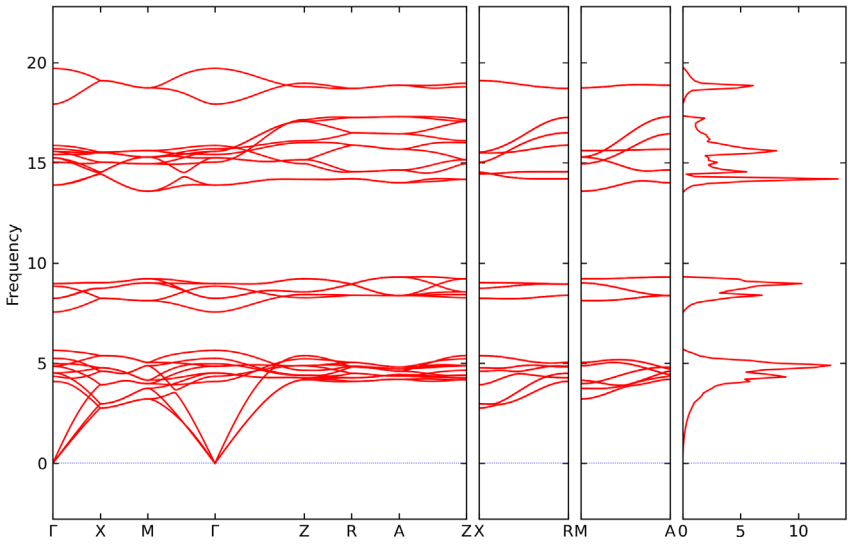

Figure S8. Phonon dispersion spectra and phonon DOS for Ta_2TiB_2.

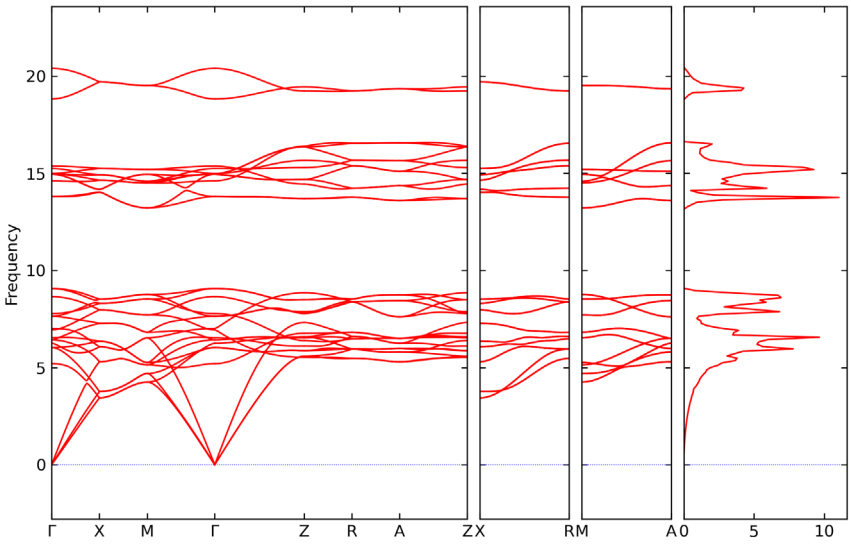

Figure S9. Phonon dispersion spectra and phonon DOS for Nb_2TiB_2.

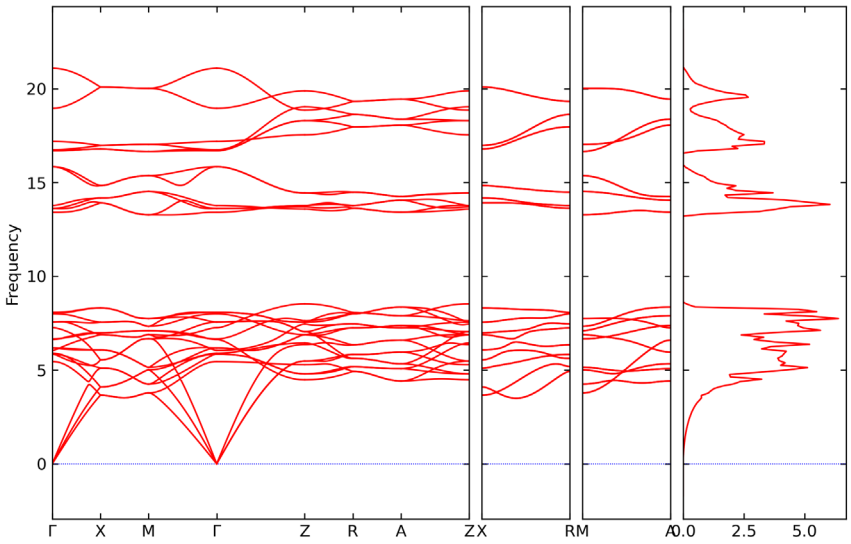

Figure S10. Phonon dispersion spectra and phonon DOS for Mo_2FeB_2.

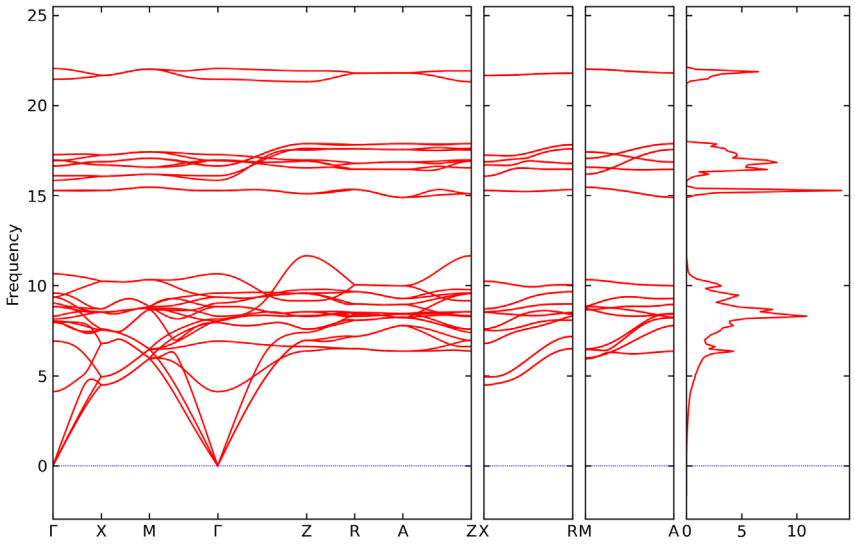

Figure S11. Phonon dispersion spectra and phonon DOS for Ti_2MnB_2.

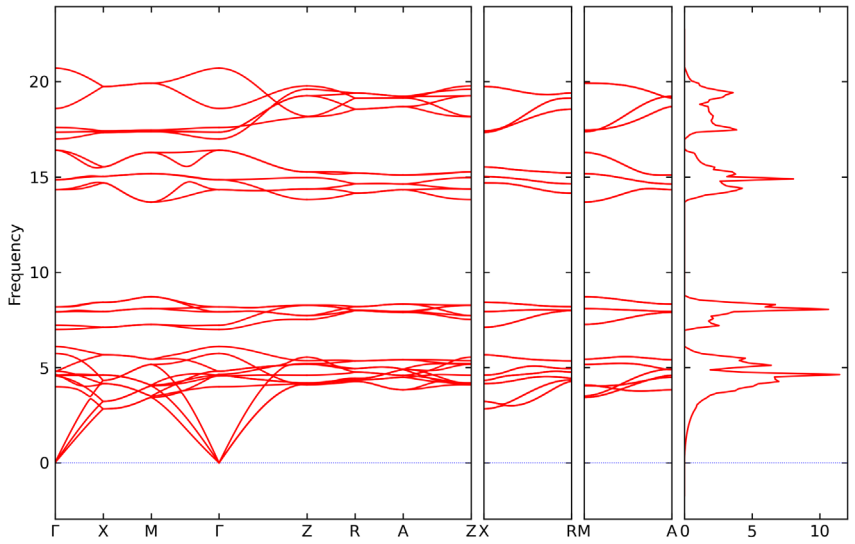

Figure S12. Phonon dispersion spectra and phonon DOS for W_2MnB_2.

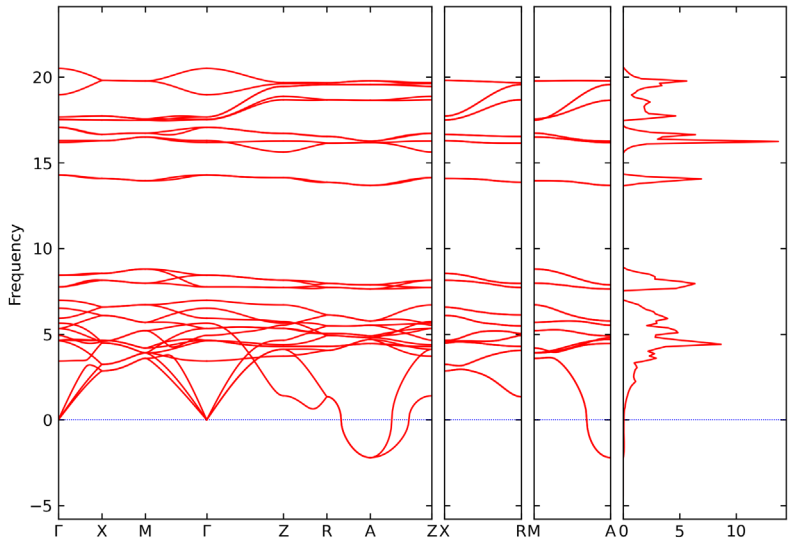

Figure S13. Phonon dispersion spectra and phonon DOS for Ta_2MnB_2. Presence of imaginary frequencies indicate dynamical unstable structure.

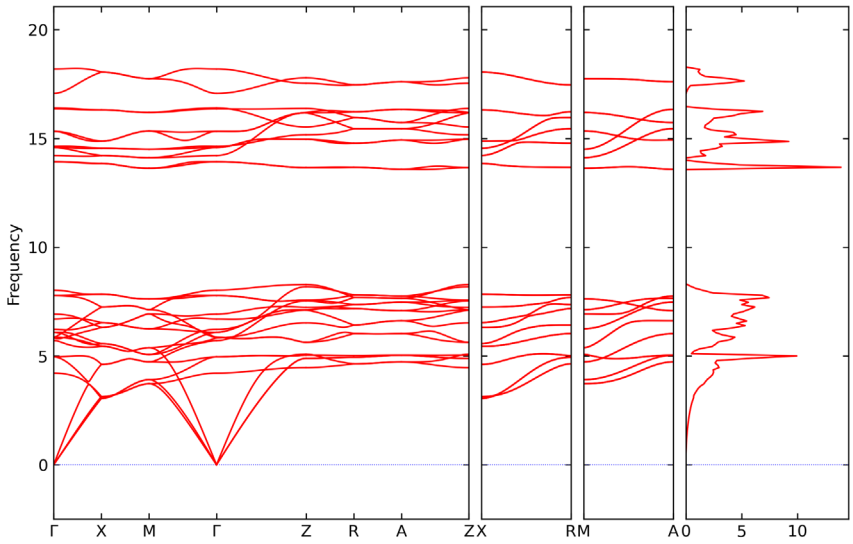

Figure S14. Phonon dispersion spectra and phonon DOS for Nb_2TaB_2.

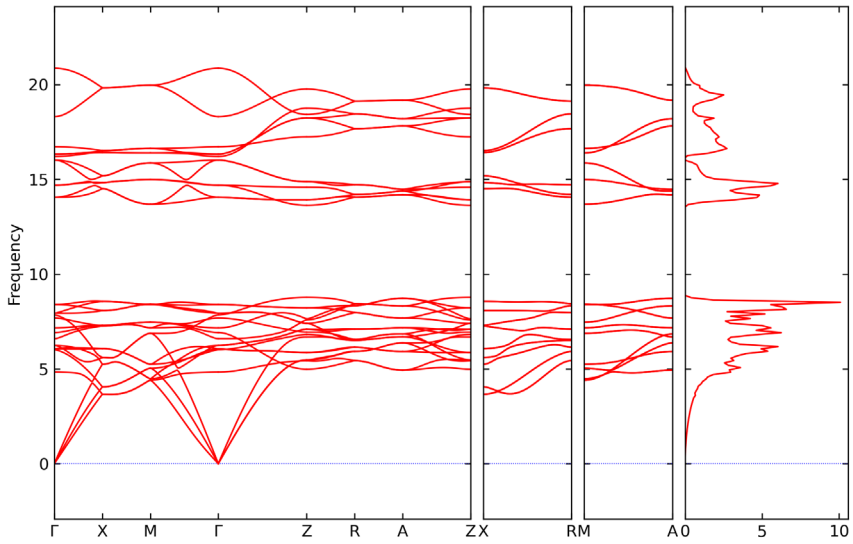

Figure S15. Phonon dispersion spectra and phonon DOS for Mo_2MnB_2.

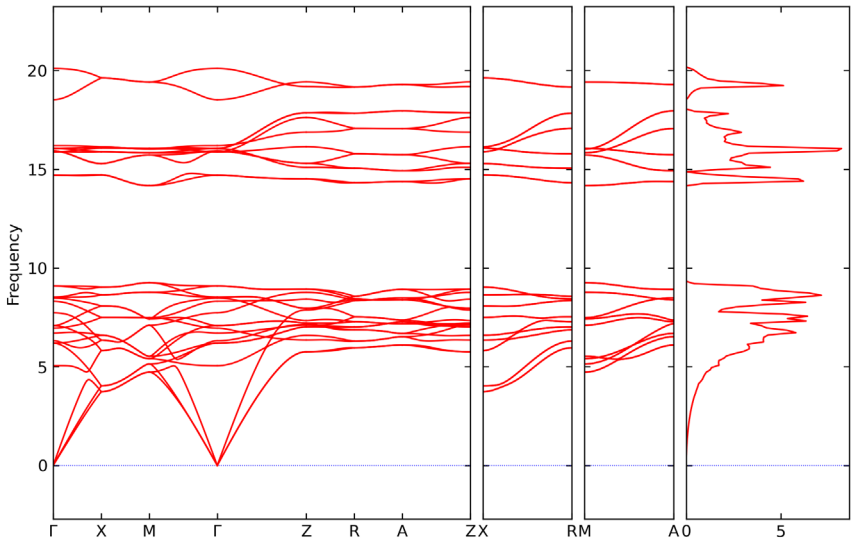

Figure S16. Phonon dispersion spectra and phonon DOS for Nb_2VB_2.

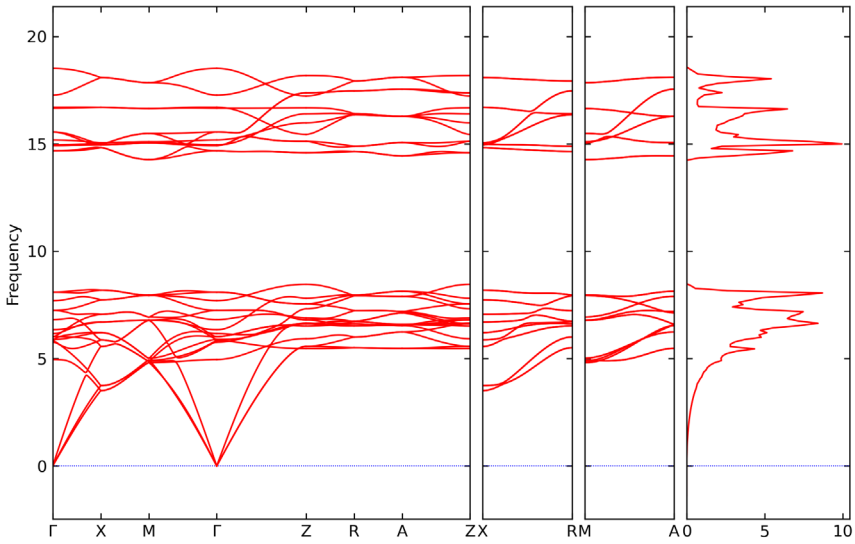

Figure S17. Phonon dispersion spectra and phonon DOS for Nb_2MoB_2.

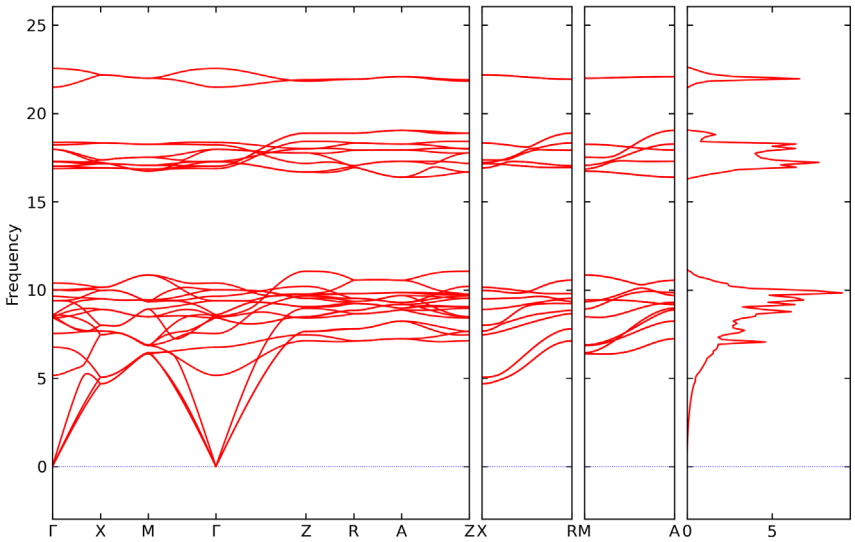

Figure S18. Phonon dispersion spectra and phonon DOS for V_2CrB_2.

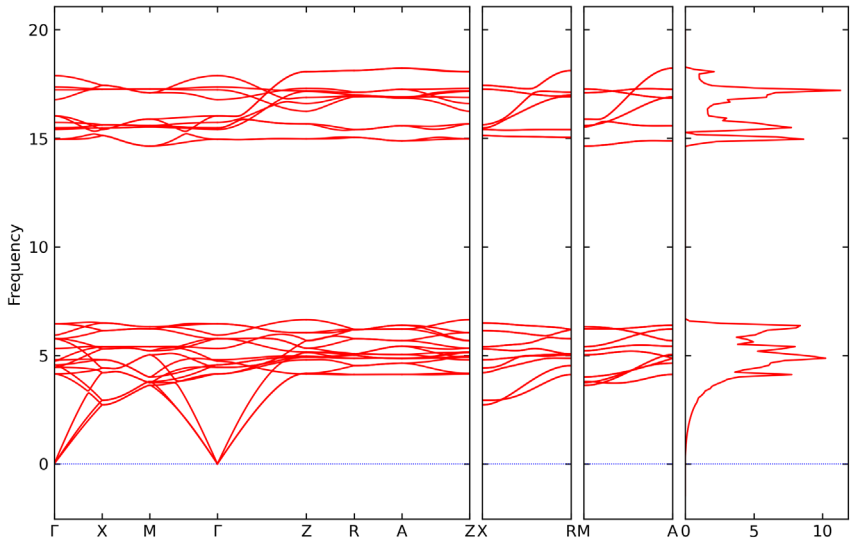

Figure S19. Phonon dispersion spectra and phonon DOS for Ta_2WB_2.

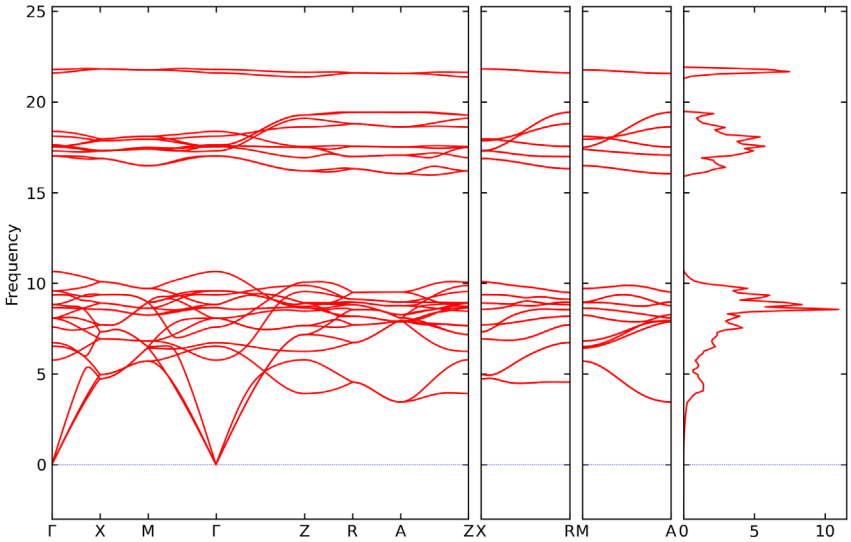

Figure S20. Phonon dispersion spectra and phonon DOS for V_2MnB_2.

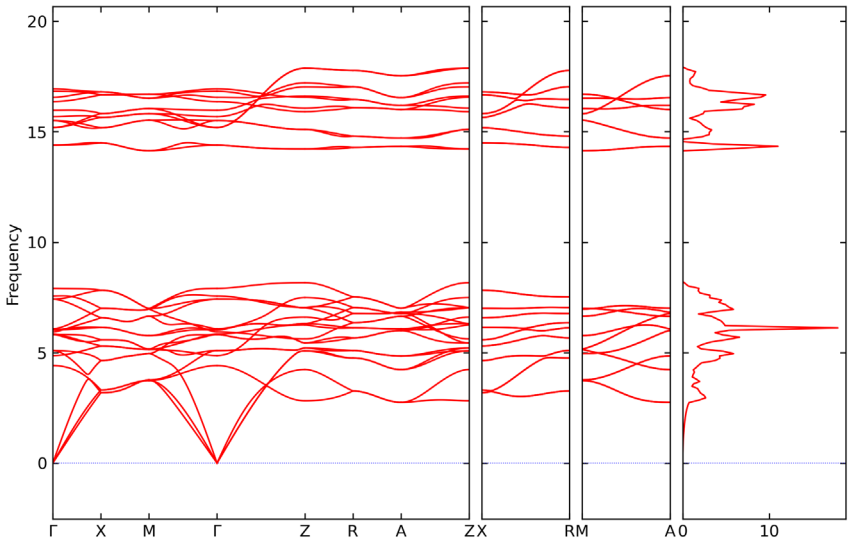

Figure S21. Phonon dispersion spectra and phonon DOS for Nb_2ReB_2.

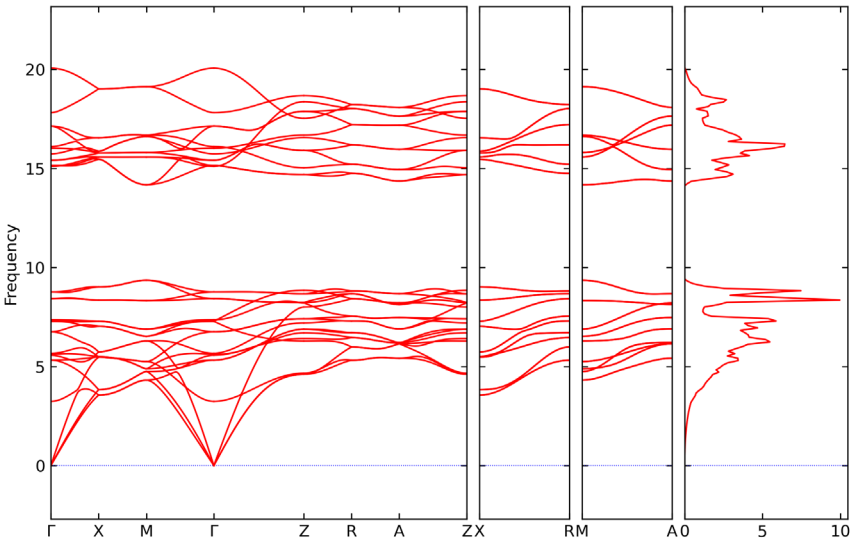

Figure S22. Phonon dispersion spectra and phonon DOS for Mo_2VB_2.

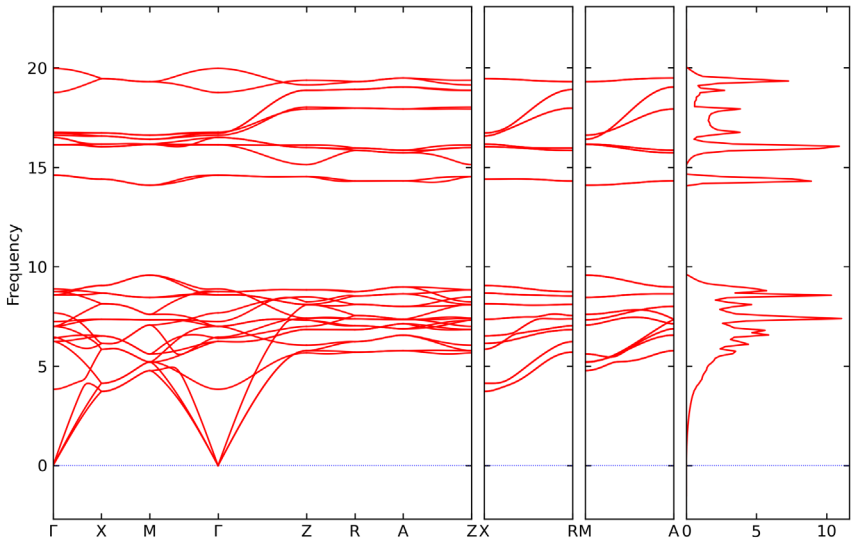

Figure S23. Phonon dispersion spectra and phonon DOS for Nb_2CrB_2.

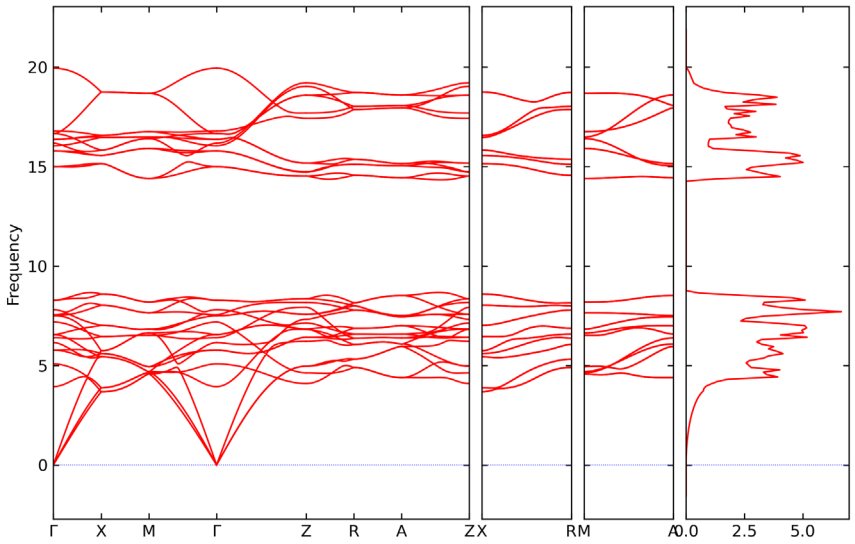

Figure S24. Phonon dispersion spectra and phonon DOS for Mo_2CrB_2.

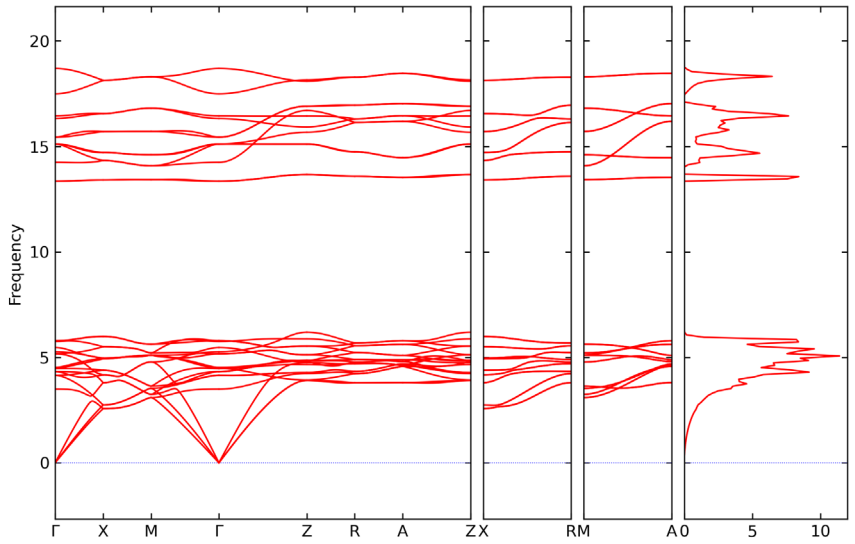

Figure S25. Phonon dispersion spectra for Hf_2ReB_2.

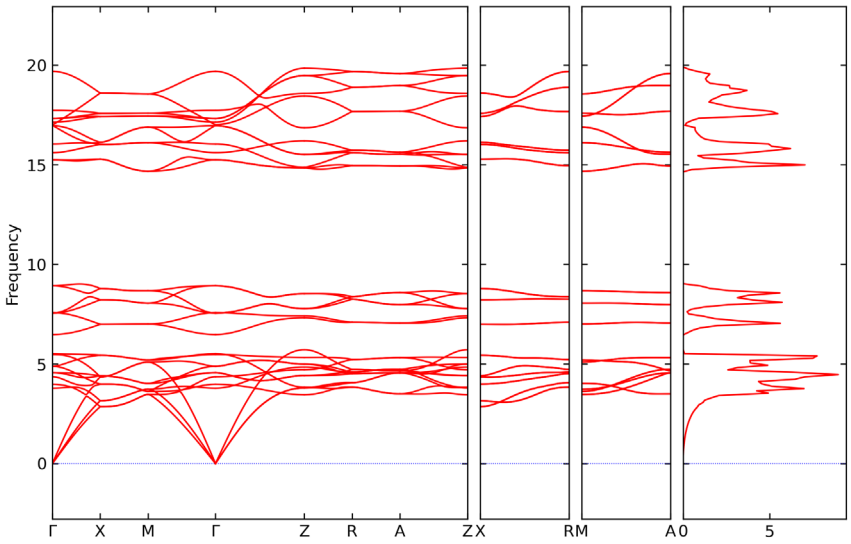

Figure S26. Phonon dispersion spectra for W_2CrB_2.

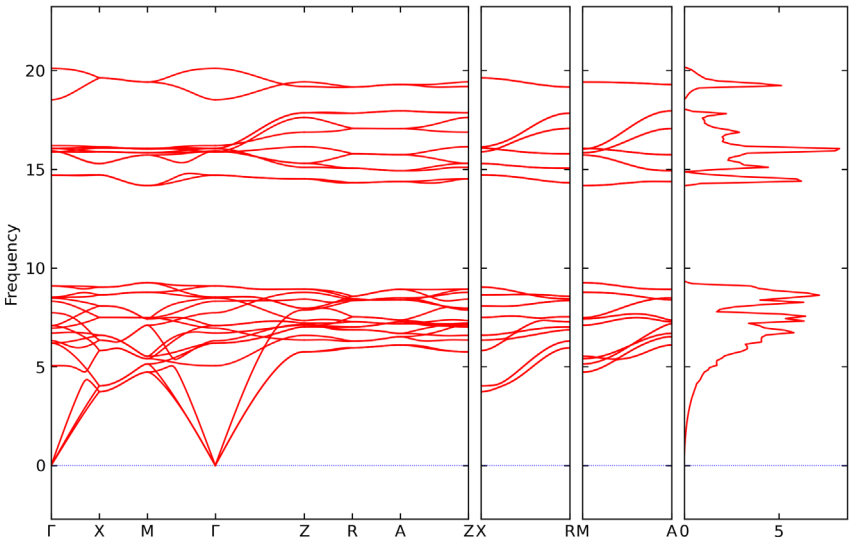

Figure S27. Phonon dispersion spectra for Nb_2VB_2.

Complete phase stability for $M'_4M''B_3$

Complete heatmap for the $M'_4M''B_3$ composition with M' and M'' being occupied by elements ranging from period 3 to 6 arranged after their atomic number. The colors range from red (metastable) to blue (stable) whereas grey illustrates phases with ΔH_{cp} > 150 meV/atom. The symbols of the elements illustrate the arrangement of the M-sublattice with a filled representing ordered and unfilled disordered. Experimentally known phases are distinguished by a black edge.

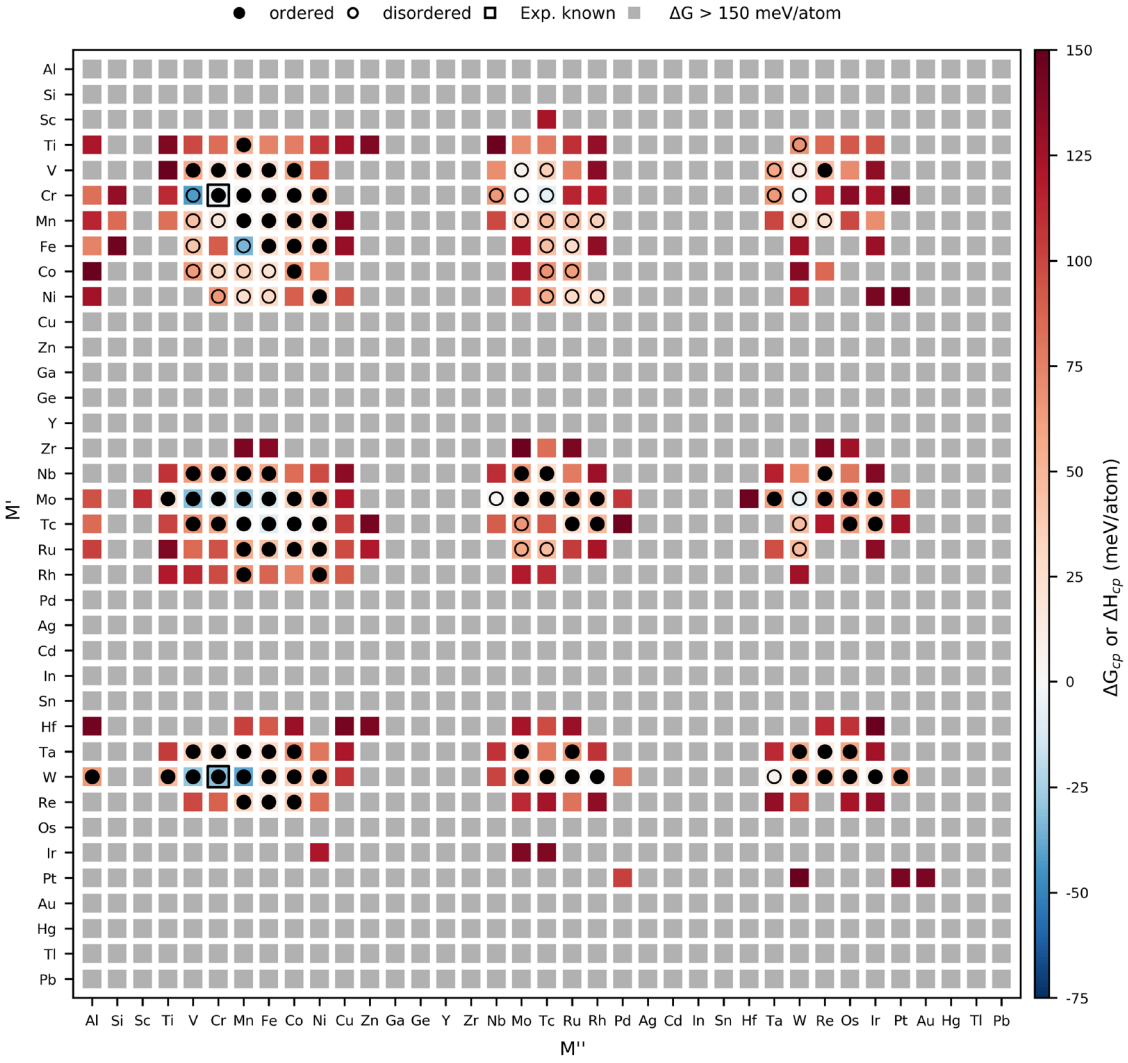

Figure S28. Complete phase stability heatmap at 2000 K where stability is depicted as the color ranging from red (metastable) to blue (stable). Phases with ΔH_{cp} > 150 meV/atom are colored grey and denoted unstable.

Table S2. Gibb's free energy, M' and M" arrangement and the set of most competing phases for the predicted stable $M'_4M''B_3$ phases with symmetry *I*4/*mcm* are displayed in Figure 3 at 2000 K.

M'	M"	ΔH_{cp} or ΔG_{cp} (meV/atom)	M' and M" arrangement	set of most competing phases
Cr	V	-42.2856	Disordered	Cr_2B + VB
W	Mn	-39.2617	Ordered	W_2B + MnW_2B_2
Fe	Mn	-34.1583	Disordered	Fe_2B + FeB + Mn_2B
Mo	V	-32.0671	Ordered	Mo + MoB + VB
W	Cr	-31.1476	Ordered	W_2B + CrB
W	V	-29.7659	Ordered	W_2B + VB
Mo	Mn	-26.3861	Ordered	Mo + MoB + Mn_2B
Mo	Fe	-10.1717	Ordered	Fe + Mo + MoB
Mo	Cr	-10.0398	Ordered	$CrMo_2B_2$ + Mo + MoB
Tc	Fe	-8.93906	Ordered	Tc_7B_3 + FeB + TcB_2
Cr	Tc	-6.71052	Disordered	Cr_5B_3 + Tc_7B_3 + CrB
Mo	W	-5.75225	Disordered	Mo + MoB + W
Cr	Cr	-5.1054	Ordered	Cr_2B + CrB
Tc	Co	-1.02338	Ordered	Tc_7B_3 + TcB_2 + CoB
Cr	W	-0.25586	Disordered	Cr_5B_3 + CrB + W
Cr	Mo	-0.24018	Disordered	Cr_5B_3 + Cr_2B + $CrMo_2B_2$

Figure S29 to S35 shows phonon dispersion spectrum for stable $M'_4M''B_3$ phases with symmetry *I*4/*mcm* and with M' and M'' being ordered. We have intentionally left out Tc-based phases since Tc is very unstable and can only be made artificially. The absence of imaginary frequencies indicates that the ordered MAB phase is dynamically stable. Only 3 out of 7 $M'_4M''B_3$ phases considered fulfills this. Note that only non-magnetic and ferromagnetic spin configurations have been considered while a more in-depth analysis of phonon dispersion for various anti-ferromagnetic spin configuration may lead to dynamically stable structures.

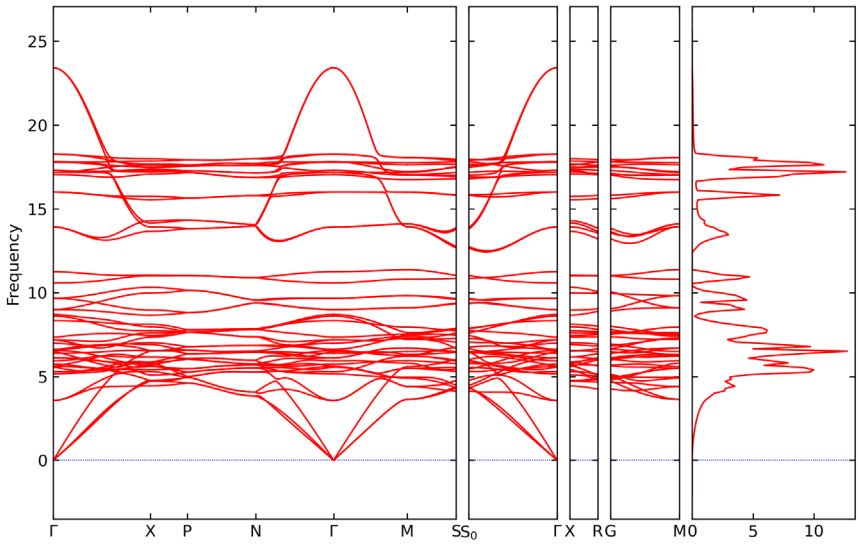

Figure S29. Phonon dispersion spectra for Mo_4VB_3.

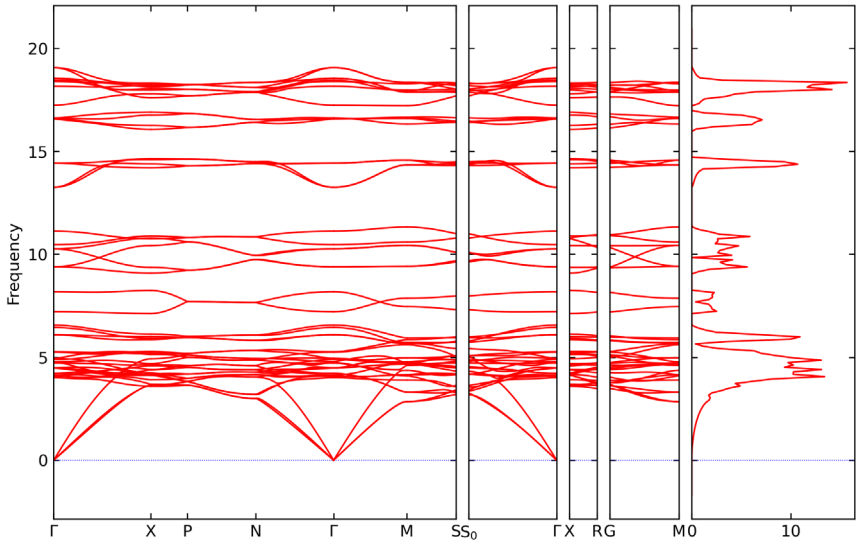

Figure S30. Phonon dispersion spectra for W_4VB_3.

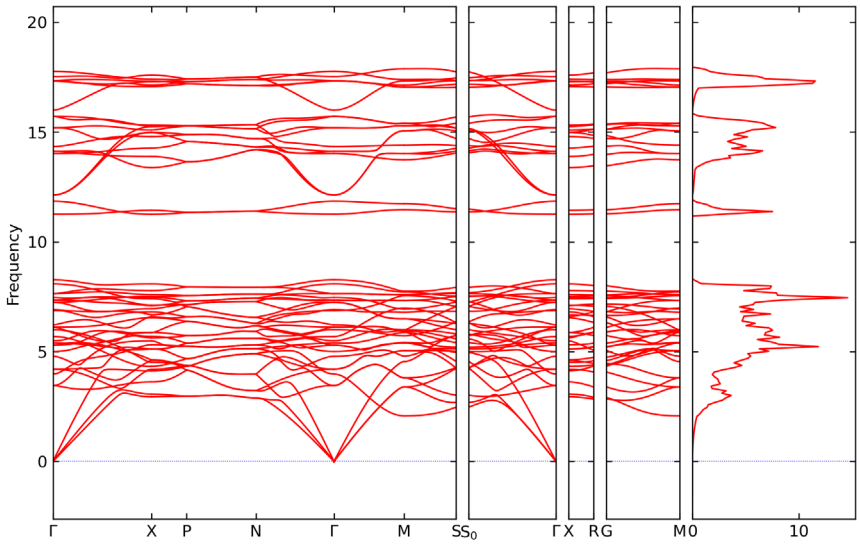

Figure S31. Phonon dispersion spectra for Mo_4FeB_3.

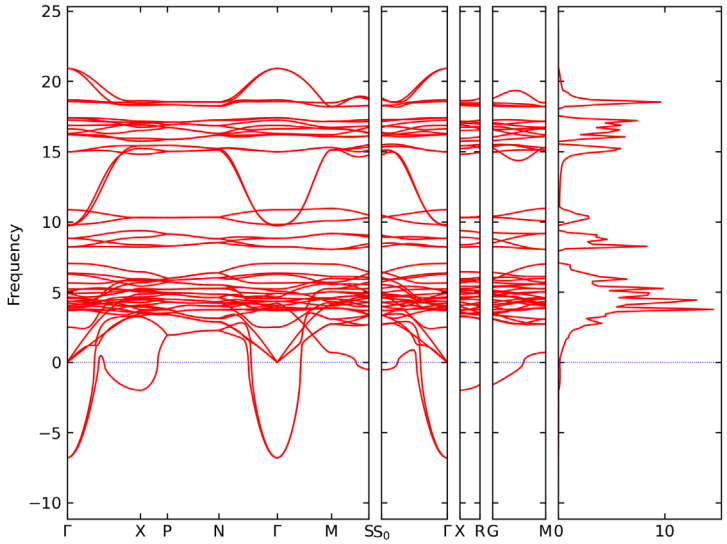

Figure S32. Phonon dispersion spectra for W_4CrB_3. Presence of imaginary frequencies indicate dynamical unstable structure.

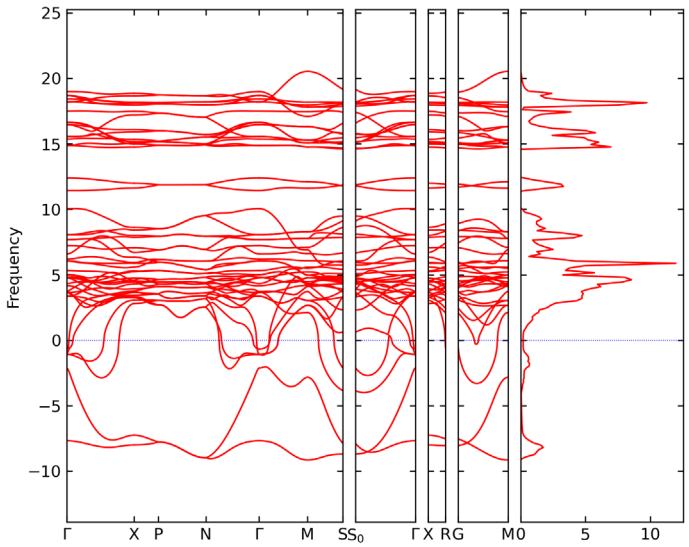

Figure S33. Phonon dispersion spectra for W_4MnB_3. Presence of imaginary frequencies indicate dynamical unstable structure.

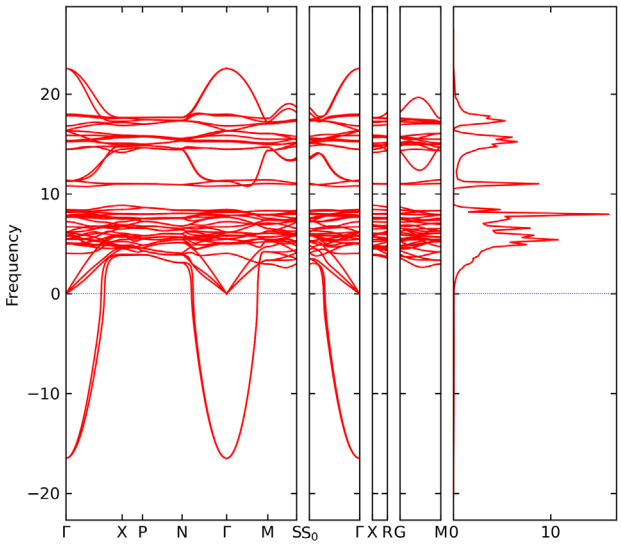

Figure S34. Phonon dispersion spectra for Mo_4MnB_3. Presence of imaginary frequencies indicate dynamical unstable structure.

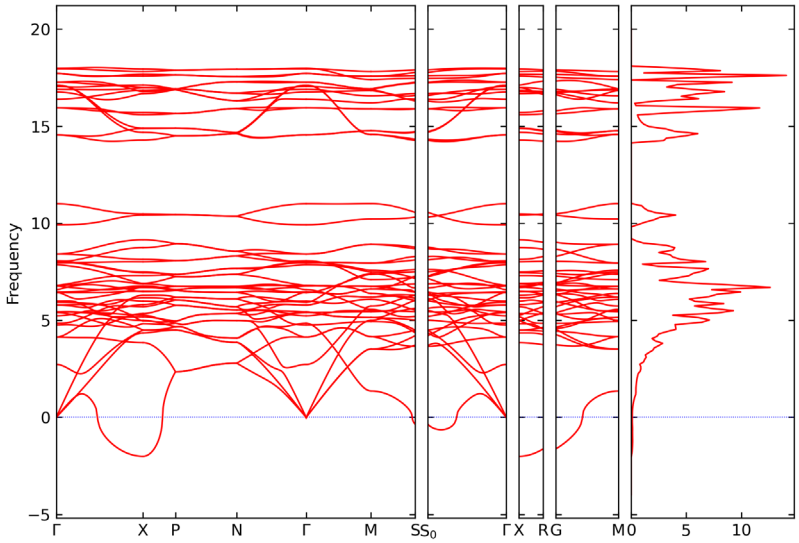

Figure S35. Phonon dispersion spectra for Mo_4CrB_3. Presence of imaginary frequencies indicate dynamical unstable structure.

Stability at finite temperatures

All stability calculations have been performed by calculating the formation enthalpy of an arbitrary M'-M''-B phase, denoted $M'_xM''_yB_z$, by comparing the energy of an arbitrary phase with the set of most competing phases at 0 K. However, the enthalpy of a material decreases with temperature due to, e.g., phonon vibrations. It has previously been demonstrated that due to a mutual cancellation of the temperature dependent energy terms, the stability at finite temperatures does not differ significantly from the calculated 0 K formation enthalpies [2,3].

The contribution from phonon vibrations to the free energy were calculated using the small displacement supercell method implemented in Phonopy [4] by applying finite displacements of 0.01 Å. The supercell for each phase was sufficiently large to converge the phonon free energy to 1 meV/atom, which was also the convergence criterion for the density of Brillouin zone mesh points for sampling the phonons. Figure S36a shows the individual vibrational phonon free energy for Ta_2TiB_2 and Ti_2ReB_2 and their set of most competing phases. Note that the vibrational free energy decreases significantly with temperature.

Next we look at the formation Gibbs free energy which is the difference in Gibbs free energy of $M'_xM''_yB_z$ with respect to the Gibbs free energy of its competing phases. Figure S36b shows the formation Gibbs free energy as function of temperature for four different $M'_2M''B_2$ phases of relevance for this work. In comparison, corresponding 0 K formation enthalpies are included as reference. Only minor changes are observed with temperature, thus demonstrating that the contribution from phonon vibrations at finite temperature mostly cancel one another for chemically similar material and further supports the approximation of only using 0 K energy terms when calculating the formation enthalpy.

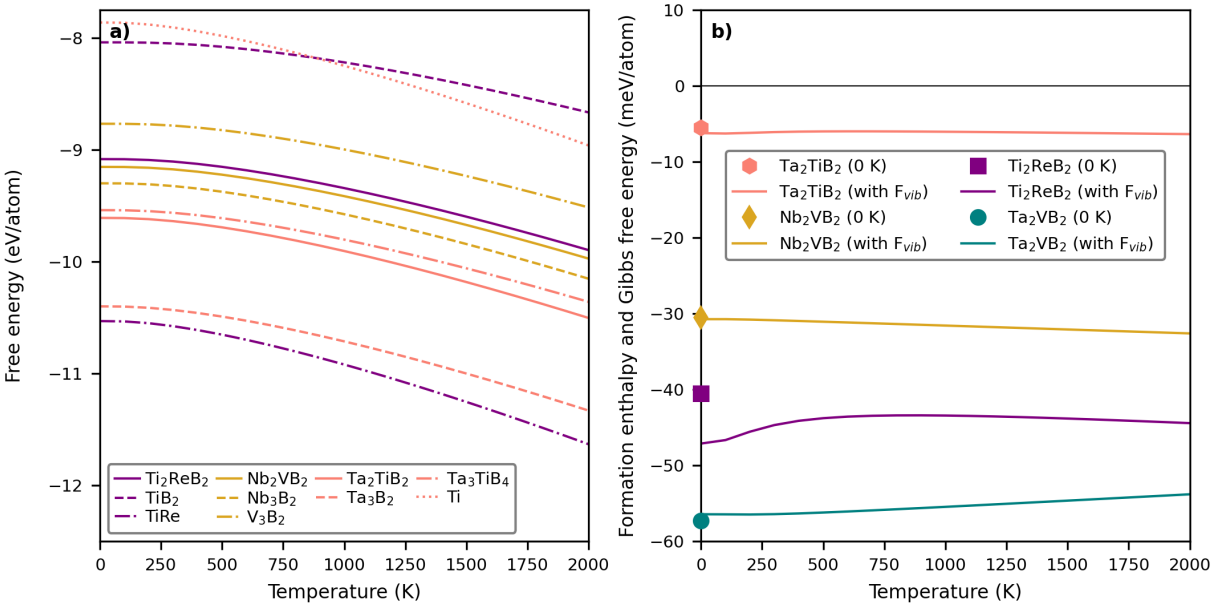

Figure S36. (a) Individual vibrational phonon free energy and (b) formation Gibbs free energy as function of temperature.

Simulated XRD patterns

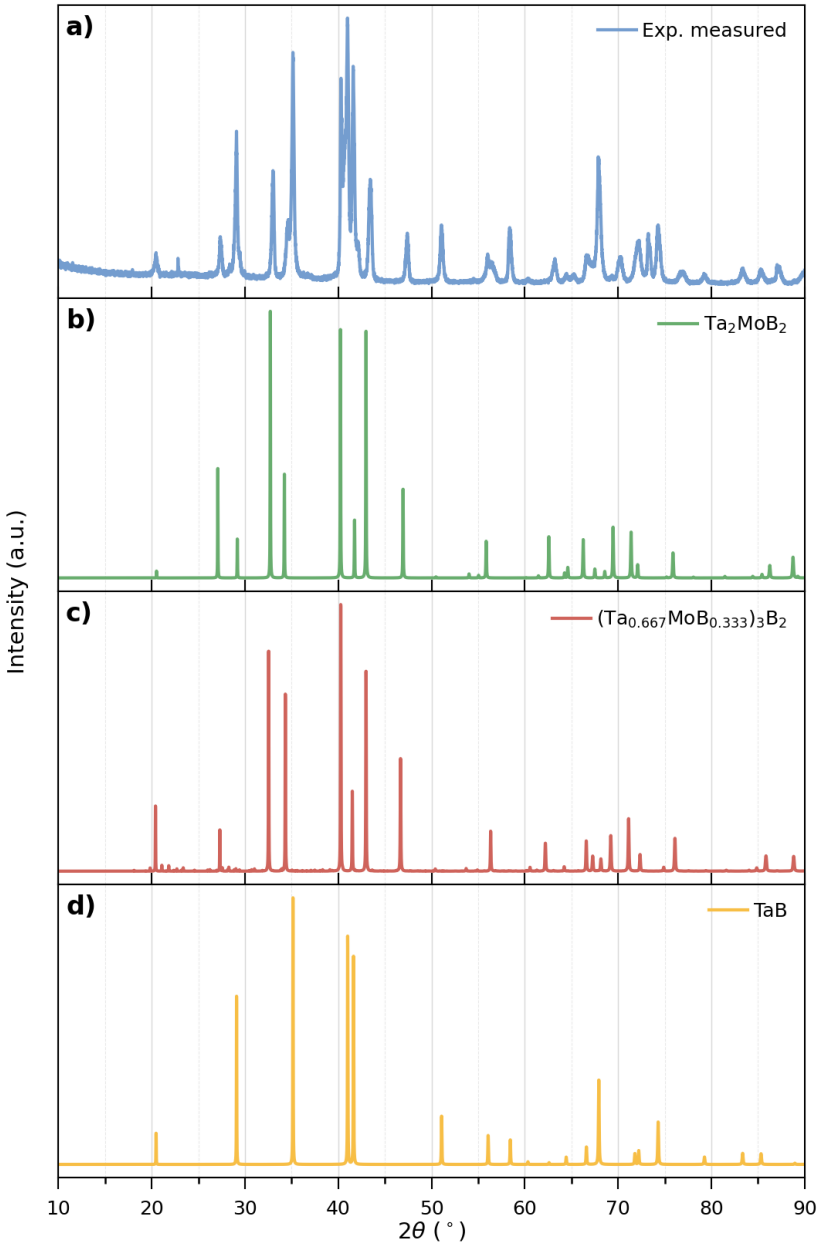

Figure S37. (a) Measured XRD pattern compared to simulated pattern of (b) ordered Ta_2MoB_2, (c) disordered $(Ta_{0.66}Mo_{0.33})_3B_2$, and (d) TaB.

SEM images

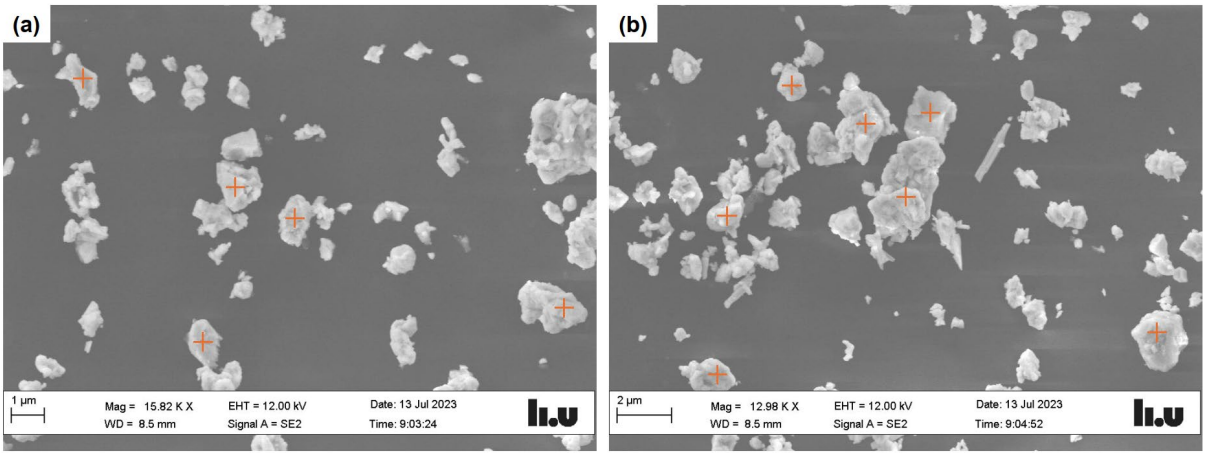

Figure S38. Representative SEM images. Orange crosses represent particles analyzed with EDX.

EDX measurements

Table S3: EDX Measurements of Ta and Mo (at%) and their calculated ratio for different particles of the Ta_2MoB_2 phase (TaB_2 particles are not shown).

Mo at%	Ta at%	Ta/Mo ratio
25.33	74.67	2.9
27.17	72.83	2.7
35.16	64.84	1.8
36.83	63.17	1.7
38.05	61.95	1.6
38.14	61.86	1.6
40.83	59.17	1.4
43.33	56.67	1.3
43.97	56.03	1.3
45.43	54.57	1.2
46.75	53.25	1.1
50.37	49.63	1.0
54.96	45.04	0.8

Supplementary References

[1]. X.B. Hu, H.Y. Niu, X.L. Ma, A.R. Oganov, C.A.J. Fisher, N.C. Sheng, J.D. Liu, T. Jin, X.F. Sun, J.F. Liu, Y. Ikuhara, Atomic-scale observation and analysis of chemical ordering in M_3B_2 and M_5B_3 borides, Acta Mater., 149 (2018) 274-284.

[2]. A. Thore, M. Dahlqvist, B. Alling, J. Rosén, Temperature dependent phase stability of nanolaminated ternaries from first-principles calculations, Comput. Mater. Sci., 91 (2014) 251-257.

[3]. A. Poulou, T.A. Mellan, M.W. Finnis, Stability of Zr-Al-C and Ti-Al-C MAX phases: A theoretical study, Phys. Rev. Mater., 5 (2021) 033608.

[4]. A. Togo, I. Tanaka, First principles phonon calculations in materials science, Scripta Mater., 108 (2015) 1-5.